ARTICLE

Effects of Dispersion Conditions of Single-Walled Carbon Nanotubes on the Electrical Characteristics of Thin Film Network Transistors

Soumendra N. Barman, Melburne C. LeMieux, Jaeyeon Baek, Rut Rivera, and Zhenan Bao*

Department of Chemical Engineering, Stanford University, Stanford, California 94395

ABSTRACT To facilitate solution deposition of single-walled carbon nanotubes (SWNTs) for integration into electronic devices they need to be purified and dispersed into solutions. The vigorous sonication process for preparing these dispersions leads to large variations in the length and defect density of SWNTs, affecting the resulting electronic properties. Understanding the effects of solution processing steps can have important implications in the design of SWNT films for electronic applications. Here, we alter the SWNTs by varying the sonication time, followed by deposition of sub-monolayer SWNT network films onto functionalized substrates. The corresponding electrical performance characteristics of the resulting field effect transistors (FETs) are correlated with SWNT network sorting and morphology. As sonication exposure increases, the SWNTs shorten, which not only affects electrical current by increasing the number of junctions but also presumably leads to more defects. The off current of the resulting transistors initially increased with sonication exposure, presumably due to less efficient sorting of semiconducting SWNTs as the defect density increases. After extended sonication, the on and off current decreased because of increased bundling and fewer percolation pathways. The final transistor properties are influenced by the nanotube solution concentration, density, alignment, and the selectivity of surface sorting of the SWNT networks. These results show that in addition to chirality, careful consideration of SWNT dispersion conditions that affect SWNT length, bundle diameter, and defect density is critical for optimal SWNT-FET performance and potentially other SWNT-based electronic devices.

KEYWORDS: single-walled carbon nanotube • network transistor • self-sorting • solution processing • sonication • percolation

Single-walled carbon nanotubes (SWNTs) have attracted much attention because of their extraordinary mechanical and electronic properties. Potential applications (1) in diverse fields, such as transistors (2, 3), transparent conducting electrodes (4), supercapacitors (5), and sensors (6−8), have been demonstrated in the laboratory. However, their commercial use has been limited to mostly structural applications instead of electronic devices. The major obstacles to integration in electronic devices are difficulties in the purification, chirality control, and controlled assembly of this nanomaterial. While some of these challenges have been partially solved with various improved vapor deposition growth processes (9), ubiquitous use of SWNTs requires solution processable methods.

Our work focuses on room-temperature solution processed SWNT network field effect transistors (FETs). Networks of SWNTs have been widely explored for electronic applications due to their ease of fabrication (10, 11). These previous reports typically used an unaligned, unsorted networks, and altered electrical percolation through the networks by careful control of SWNT density. While this random architecture allows for facile processing and scalability, device performance is compromised when compared to individual SWNTs, primarily because of the mixture of metallic and semiconducting SWNTs and resistance at tube−tube junctions. To improve on random SWNT networks, aligned SWNT networks have been grown in CVD processes on quartz and sapphire substrates and can be subsequently transferred onto other surfaces (12, 13). Although there have been refinements to this process including removal of stripes (14) and optimization of growth conditions (15), there still exist metallic tubes in the transistor channel. Density gradient centrifugation (DGU) has been used to isolate surfactant wrapped nanotubes of selective diameters and chiralities (16). This method can be utilized to create solutions consisting of primarily semiconducting SWNTs (17, 18). However, the surfactants adsorbed onto the SWNT walls are difficult to remove completely and may degrade electronic properties.

Surface sorting is a process developed in our laboratory for preparing partially aligned semiconducting or metallic SWNT networks from solutions at ambient conditions (2). SWNT chirality selection and alignment is achieved in an one-step solution deposition process by controlling substrate surface chemistry and spin coating speed (19). However, to ensure efficient sorting, a dispersion of pristine SWNTs with minimal bundling is critical. The as-grown SWNTs contain many impurities, such as metal catalysts and amorphous carbon, and need extensive purification before they are suitable for electronic applications. In addition, strong van der Waals interactions between nanotubes render unfunc-

* Corresponding author. E-mail: zbao@stanford.edu. Phone: (650) 723-2419. Fax: (650) 723-9780.
Received for review June 16, 2010 and accepted August 16, 2010

DOI: 10.1021/am1005223

Published on Web 08/25/2010

tionalized SWNTs insoluble in common solvents. Therefore, SWNTs usually aggregate into bundles of many nanotubes containing both semiconducting and metallic SWNTs. Structural applications may benefit from having bundles; however, for high performance electronic applications, the mixture of chiralities results in degraded transistor properties because of shorting or increased off current from metallic SWNTs.

To solubilize SWNTs into a stable dispersion in water or organic solvents, a myriad of solvents (20, 21) and surfactants (22) have been reported. Various molecules such as DNA (23), polymers (24), and ionic liquids (25) have also been utilized for solubilization. Acid treatments (26), and covalent functionalization techniques (27, 28) may also be used to impart solubility, however, these processes dramatically alter SWNT optical and electronic properties. Previous work by other groups have shown that an ideal organic solvent for SWNT dispersion should have a high tendency for electron pair donation and a negligible value of hydrogen bond donation, and should be slightly basic (29). We have chosen to disperse SWNTs in *N*-methyl-2-pyrrolidone (NMP) because it has been shown not only to effectively disperse SWNTs (30), but has been shown to have a negative enthalpy of mixing for small diameter SWNTs, resulting in individualized nanotubes (31). Even though various methods for dispersion have been studied extensively, little is known about the effects of dispersion conditions, such as sonication power and time, on surface sorting and the resulting electronic properties of devices.

In this paper, we investigate the effects of solution dispersion conditions on surface sorting and the corresponding self-sorted SWNT network field effect transistors. We systematically vary the sonication time for dispersion and examine the effect on solution concentration, SWNT length, and degree of bundling. These parameters in turn impact the surface sorting, adsorbed SWNT density, and alignment and eventually the overall device performance.

EXPERIMENTAL PROCEDURE

Highly purified arc-discharge SWNTs were purchased from Hanwha Nanotech (SWNT, ASP-100F). The as-prepared SWNTs were dispersed at a concentration of approximately 5 μg/mL in 200 mL of *N*-methyl-2-pyrrolidone (NMP) (Fisher Scientific) by sonication at 225 W (Cole Parmer, Ultrasonicator Processor CP 750). Aliquots (2 mL) were sampled at various times during sonication. For batch 1, samples were taken at 10, 20, 30, 40, 60, 90, 120, 180, and 240 min. For batch 2, samples were taken at 10, 20, 30, 45, 60, 90, 120, 150, 180, 210, 240, 300, 360, 420, and 480 min. An ice and water bath was used to keep the solution from overheating. Following sonication, the solutions were centrifuged at 15 000 rpm (SORVALL RC 5C Plus, SW-34**)** for 90 min to remove large bundles and other impurities. Solution characterization was performed on a Cary 6000i UV−Vis−NIR spectrophotometer using a 1 cm wide quartz cuvette. The as-purchased NMP was used for background absorption correction. Piranha cleaned (Caution: Piranha solution is highly energetic and corrosive!) heavily doped silicon substrates with 300 nm of thermally grown dry oxide (2.5 cm × 1 cm) were placed in a 0.5% v/v solution of aminopropyltriethoxysilane (APTES) in anhydrous toluene for 40 minutes inside a dry N_2 glove box, followed by 3 rinses with anhydrous toluene. Contact angle goniometry was used to measure the contact angle of the APTES monolayer (∼CA = 65° ± 2°) as a quick method to verify the quality of the self-assembled monolayer (SAM). A SWNT solution (400 μL for batch 1 and 330 μL for batch 2) was dispensed drop wise (Headway Research spin-coater) onto the center of an APTES-functionalized SiO_2 wafer at 4000 rpm, and then dried in a vacuum oven at 120 °C for 1.5 h. A syringe pump was used to precisely deliver the SWNT solution at a rate of 60 μL/min to the spinning wafer during the deposition step.

An atomic force microscope (AFM) (Digital Instruments, model 401) was used to characterize the morphology and density of the surface adsorbed SWNTs. Care was taken to image the same region of each wafer along the center line ∼0.5 cm from the short edge of the wafer. Image-Pro (Media Cybernetics) and ImageJ (NIH) software was used to obtain statistics on the density, length and alignment from 5.0 μm × 5.0 μm scans. Bundle heights were obtained by using sectional analysis of 2.5 μm × 2.5 μm images using the NanoScope (Digital Instruments) software. Field effect transistors (FETs) were made via thermal evaporation of gold source and drain electrodes (40 nm) through a shadow mask placed on the SWNT coated functionalized Si/SiO_2 wafers. The resulting SWNT-FETs had channels of 50 μm in length and 1 mm in width. Electrical characterization was performed using a semiconductor parameter analyzer, (Keithley, Model 4200) with a source-drain voltage of −1 V (batch 1) or −0.1 V (batch 2) and gate voltage of 10 V to −2 V.

RESULTS AND DISCUSSION

To investigate the effect of solution dispersion conditions on SWNT-FET device characteristics, low concentration (∼5 μg/mL) SWNT/NMP solutions were prepared by sonication. Sonication has been shown to de-bundle and at the same time shorten SWNTs (32). Therefore, sonication time and power determine the SWNT concentration, degree of bundling, length, and defect density; all of which should affect transistor properties. High-concentration solutions usually contain bundles (31), which contain a mix of semiconducting and metallic SWNTs resulting in primarily metallic conduction through the bundle and which can cause shorting of the SWNT-FETs. Long SWNTs are desirable for both thin film transistor (TFT) applications and conducting films as they can potentially reduce the number of tube−tube junctions in the SWNT network (33), which are the primary source of resistance. Extensive sonication cuts SWNTs into shorter segments (34) and introduces defects on the SWNTs, which can scatter charge and further decreases conductivity.

UV−Vis Spectroscopy. Aliquots (2 mL) of SWNT solutions were sampled at different time intervals during sonication and subsequently centrifuged to remove larger bundles. A convenient way to observe the effect of sonication and centrifugation is UV−vis−NIR spectroscopy. Interband transitions between van Hove singularities in the density of states can be observed in optical absorption spectroscopy. Figure 1A plots the peak intensity of the E^{M}_{11} transition peak at 692 nm after centrifugation as a function of sonication time. This peak is a prominent feature in the spectra in a region where there should not be any background absorption. Batch 1 showed a lower absorption than batch 2, primarily because of weighing error for milligram quantities of nanotube powder. However, the observed

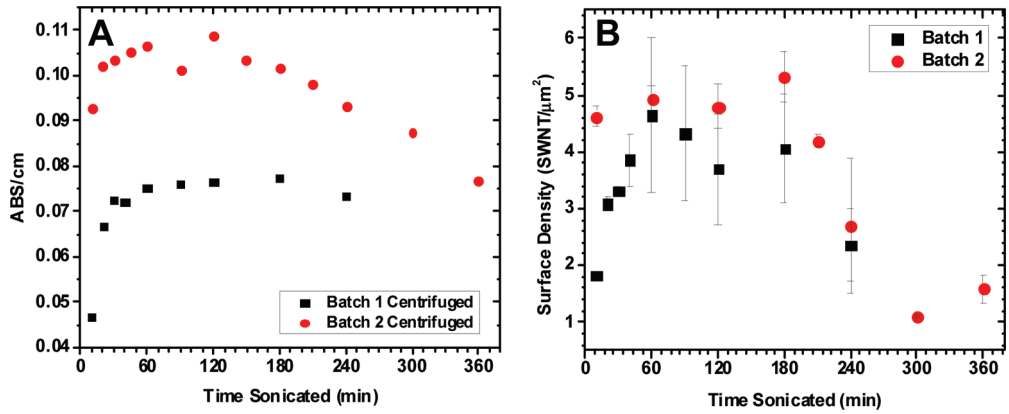

FIGURE 1. (A) Absorbance at 692 nm for solutions after centrifugation increased with time and the decreased after 120 to 180 min of sonication. (B) SWNT surface density from AFM data follows a similar trend as the solution absorbance.

trends discussed in this section and later sections are consistent, showing the general trend is reproducible. The absorption intensity for both batches increased from 10 to 30 min as the energy from sonication broke up large bundles allowing more SWNTs to disperse into solution. The absorption intensity slowly increased and peaked at 120 to 180 min depending on the initial solution concentration.

The optical absorption of the centrifuged solution decreased after 120 to 180 min of sonication due to increased bundling as evidenced from analysis of atomic force microscopy (AFM) images discussed in the next section. This may be a result of increased water absorption from air by the polar NMP solvent after extensive exposure in air. This hypothesis is supported by the observation that some absorption features above 1000 nm in the spectra increased with longer sonication times. They matched the peaks found when water was added to NMP (Figure SI-1A) and were attributed to water absorbed from the environment into the hygroscopic NMP during sonication (30). The addition of water into NMP/SWNT solutions has been shown to cause the bundling of SWNTs (35). After extended sonication, more SWNT bundles were present and after centrifugation the concentration of individualized SWNTs and smaller bundles was lower accounting for the lower absorption intensities. We found a similar increase in background absorption and in the NIR region for a neat NMP sonicated without SWNTs (see Figure SI-1B in the Supporting Information) and the color of NMP became yellow after extended sonication. Oxidation (36) and heat-induced (37) reactions in NMP have been reported in the literature. Even though this solution was placed in an ice bath, bubble cavitation created by sonication could locally heat and introduce radical species, which could cause NMP to react and form other species or even polymerize.

Spectroscopic evidence for shortening and debundling of the SWNTs in the centrifuged solutions is provided in Figure 2 where the absorption spectra blue-shifts with increasing sonication time. SWNTs extracted from density gradient ultracentrifugation optimized for length separation also showed this blue-shifting with shorter SWNTs (38), and aggregation of SWNTs into bundles was correlated with a red shift of the spectra (32). Therefore, the observed blue

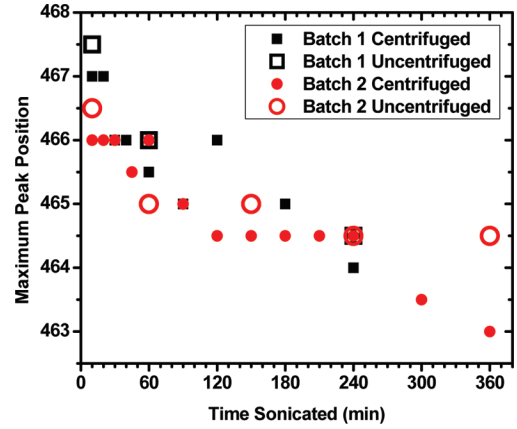

FIGURE 2. Blue shifting of the E^{S}_{33} absorption peak centered around 466 nm due to debundling and shortening of SWNTs with increased sonication time. The peak position for centrifuged solutions are blue-shifted compared to uncentrifuged peaks with the same sonication time.

shift is consistent with SWNT shortening and increased debundling with increased sonication time. Also, the spectra of centrifuged solutions are blue-shifted when compared to the uncentrifuged solutions, indicating the removal of large bundles from the solution.

The absorption coefficient of a solution sonicated for 30 min at 225 W without subsequent centrifugation was 0.0192 mL/(μg cm) at 692 nm. This is lower than the value of 0.0326 mL/(μg cm) at 660 nm reported by Giordani in NMP (30) on 0.0300−0.0347 mL/(μg cm) at 700 nm reported by Landi in aminated solvents (39). We attribute this difference in optical absorption coefficients to using arc-discharge vs HiPCO SWNTs where arc-discharge SWNTs have, on average, larger diameters than HiPCO tubes.

Atomic Force Microscopy. The morphology of the deposited SWNT networks was characterized by AFM. Image analysis software was used to determine the density, length, alignment and bundle height of representative samples. The AFM images obtained from surfaces created with 10, 60, and 180 min samples from batch 1 and the 300 min sample from batch 2 are shown in Figure 3 (additional AFM images from other time points are shown in Figure SI-6 in the Supporting Information). The averaged SWNT surface density obtained from the length and bundle height analysis is plotted against

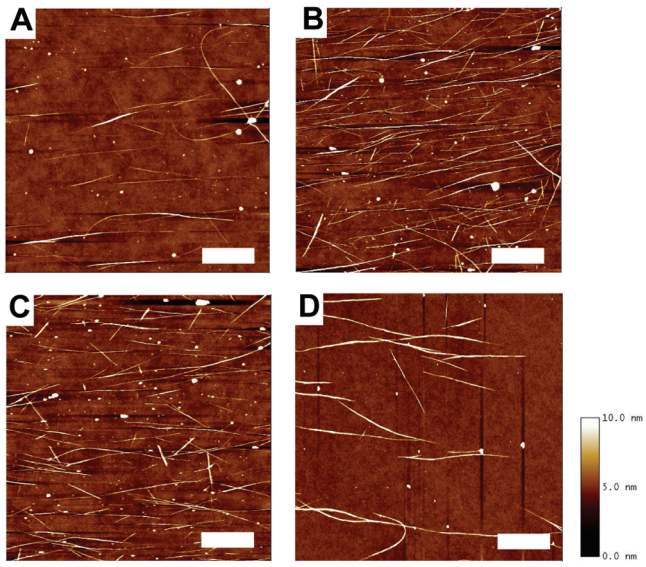

FIGURE 3. AFM images of SWNTs adsorbed via spin coating onto APTES functionalized SiO_2 wafers. (A–C) Batch 1, 10, 60, and 180 min sonication times, respectively. (D) Batch 2, 300 min sonication time. For sonication times <180 min, longer sonication times generally resulted in more surface tube density, shorter tubes, and less alignment. For times >180 min, the surfaces had more SWNT bundles and lower surface density because of sonication and water-induced solvent effects. The scale bar for all images is 1 μm. Additional images are included in the Supporting Information.

the UV–vis–NIR absorbance of solutions in Figure 1B. The solution concentration and the surface density after deposition follow similar trends of increasing initially, and then slowly decreasing with increased sonication time. The amount of solution deposited on the substrate for batch 2 was lower than batch 1, but the higher concentration in solution resulted in a slightly higher SWNT surface density for batch 2. A quantitative length analysis for batch 1 is displayed in Figure 4A with box and whisker diagrams where the bounds of the box represent the 75th and 25th percentiles of the data set, the outer whiskers show the 95th and 5th percentiles and the inner square and inner line represent the mean and median, respectively. We observed a gradual decrease in the SWNT length with extended time as well as a decrease in length polydispersity between the 25th and 75th percentiles. From Figure 4B, the height of SWNTs adsorbed on the surface corresponding to bundle diameter increased initially from 10 to 30 min. The 10 min sample has a narrower distribution and a smaller height consistent with the diameters expected for these arc-discharged SWNTs (1.4 ± 0.4 nm) (2) implying that the adsorbed SWNTS were mostly individualized SWNTs. After 30 min of sonication, there was a decrease in bundle height and polydispersity between the 25th and 75th percentiles as sonication further decreased the bundle size. This general trend was also supported by the blue shifting of UV–vis–NIR peaks discussed earlier in Figure 2. After 180 min of sonication, there are fewer individual SWNTs on the surface because of water absorption into NMP and solvent degradation by sonication as discussed earlier. Length and bundle analysis for batch 2 are presented in the Supporting Information.

Figure 5A shows the distribution of alignment vs length from batch 1 with the angles normalized to 0° as the mean of the alignment for all sonication times. There is a greater degree of alignment anisotropy in the shorter SWNTs (<1μm). The triangular shape of the distribution shows the longer SWNTs have greater alignment in the direction of the flow. The standard deviation in alignment of samples fabricated can be used as a proxy for degree of alignment. When this standard deviation is plotted against the average length of SWNTs on a substrate, the degree of alignment is greater in networks with longer SWNTs, as shown in Figure 5B. Aligned SWNT networks with a controlled amount of misalignment are critical for optimal electronic percolation (19, 40).

Electrical Characterization. The debundling of SWNTs into smaller bundles and isolated SWNTs should result in SWNT network thin film transistors (SWNT-TFTs) with higher on/off ratios. However, we noticed that it also depends on other factors, such as defects, CNT length, solution concentration, tube density, alignment, and sorting efficiency. We have made efforts to minimize the errors from processing, but even for percolating networks with the exact same density, there can be a large range of conductance (41), especially in the low density sub-monolayer

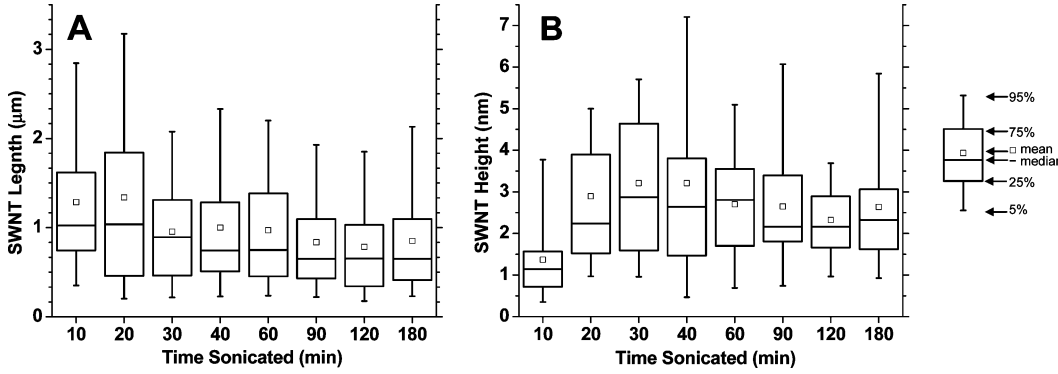

FIGURE 4. Box and whisker diagrams of SWNT length and height on functionalized surfaces as a function of sonication time for batch 1. (A) Bundle length decreased gradually with sonication time. (B) Bundle height increased at first with time until 30 min of sonication as larger bundles were broken up and debundled with increased sonication. From AFM analysis, the diameter of the arc-discharge SWNTs used are 1.4 ± 0.4 nm (2). A compromise between SWNT length, height, and surface adsorption yield occurs at 30 min. The outer whiskers of the box and whisker diagrams show the 95th and 5th percentiles of the data set. The box represents the 75th and 25th percentiles and the inner square and inner line represent the mean and median, respectively.

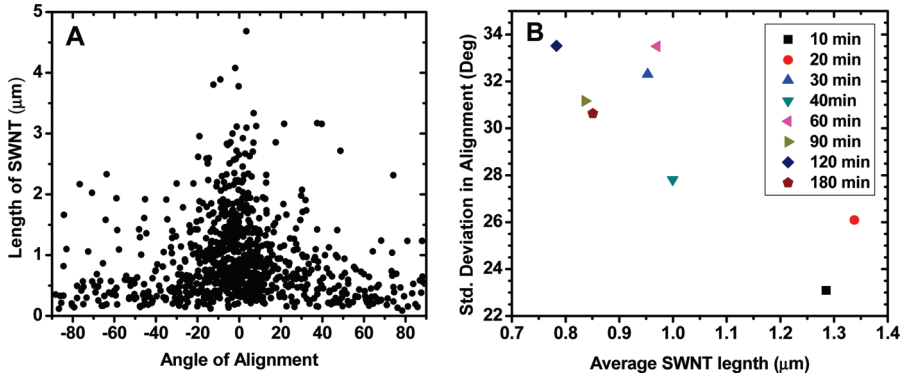

FIGURE 5. (A) SWNT alignment distribution for substrates from batch 1 as a function of SWNT length measured by AFM. Short SWNTs have the most angular anisotropy. (B) Standard deviation for the degree of alignment is plotted against the average SWNT length. The networks created from longer SWNTs have better alignment.

networks presented here However, general trends were found to be consistent with data from many devices prepared in different batches.

In panels A and B in Figure 6, box and whisker diagrams display the on and off current distribution of 9−13 transistors fabricated on the same wafer for each of the sonicated solutions. The bounds of the box represents the 75th and 25th percentiles of the data set, the outer whiskers show the 95th and 5th percentiles, and the inner line represents the mean. There appears to be two regimes present from this data: the first is dependent on concentration and surface sorting and the second in extended time range limited by solvent bundling effects. For the first time period during sonication up to 180 min, the on current is on the order of a tenth of microamp to a microamp with variations following the solution concentration and the surface density. However, the off current for these devices surprisingly increased with sonication time, resulting in decreasing on/off ratios as shown in Figure 6C.

From the percolation theory, the percolation threshold and conductivity of a network of sticks are dependent on density, alignment, length, length polydispersity among other factors. The conductivity of a percolating network has a power law relation to the density above the percolation threshold (42).

$$\sigma \approx (N - N_C)^{\alpha}$$

where σ is the conductivity, N is the SWNT density, N_C is the percolation threshold, and α depends on the dimensionality of the space, theoretically predicted to be 1.33 for two-dimensional systems and 1.94 for three-dimensional systems. The percolation threshold is dependent on the average length of the stick (L_s) and the angle of alignment.

$$N_C = f^2/\pi L_s^2$$

where f is dependent on the length and alignment distribution. It is equal to 4.236 for an isotropic network with uniform stick lengths and is 2.0 for a network with a log normal length distribution. As the length of the SWNT decreases, the percolation threshold increases. This could explain why the on current remains at the same order of magnitude even though the lengths decrease. As the sonication time increased, the SWNT surface density post-deposition increased as more SWNTs remained in solution after centrifugation while the length of the tubes decreased, resulting in a higher percolation threshold. The change in percolation threshold, however, cannot explain the increase of the off current with extended sonication time. If two surfaces have the same surface SWNT concentration but different lengths, the sample with shorter SWNTs will have a larger percolation threshold and a lower conductivity than a sample with longer SWNTs. The off current mainly depends on the contribution of the metallic SWNTs which are expected to be ∼1/3 of the SWNTs if unsorted. If the difference between density and percolation threshold stays constant as implied by the constant on current, one would expect the conductivity in the off state, where the density is ∼1/3 of the on-state density, to decrease with decreasing stick length and become less than the percolation threshold. This is the opposite of what is observed.

If the ratio of semiconducting to metallic SWNTs decreases, then there would be an increase in the off current. We have previously proposed a mechanism for chirality enrichment by surface sorting (43). Briefly, the Lewis base nature of the NMP solvent resulted in a net negative charge on the SWNT defects in solution (29). When this SWNT solution is spin-coated onto APTES-functionalized wafers, electrostatic interactions at the positively charged surface preferentially attracts larger diameter SWNTs. For the arc-discharge SWNTs used in this study, the larger diameter SWNTs are primarily semiconducting. The small curvature of the larger diameter tubes resulted in a greater interaction of carboxylic acid defects and the amine surface led to more semiconducting SWNTs adsorbing on the surface while the weaker bound metallic SWNTs fly off the substrate with excess solvent because of the hydrodynamic forces from the spin-coating process. Sonication has been shown to cut SWNTs as well as increase the amount of defects on SWNT surfaces. The smaller diameter SWNTs have a larger bond strain because of increased curvature (44) and would be more likely to have sonication introduced defects. With

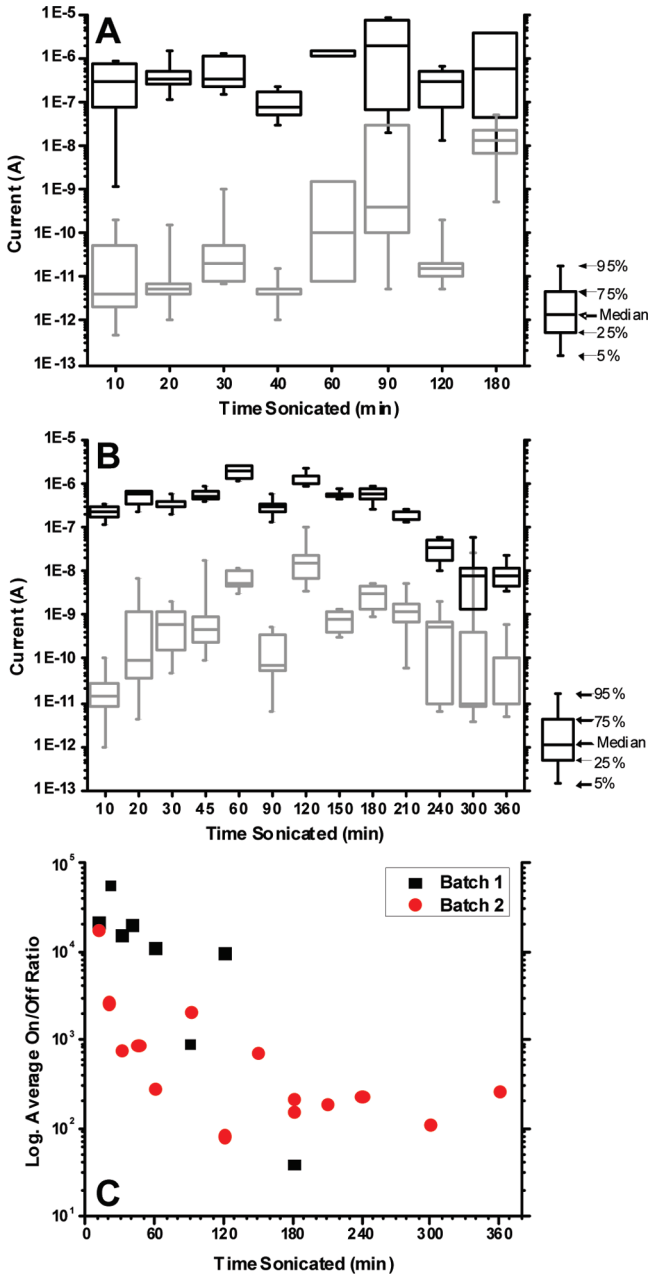

FIGURE 6. Electrical data from SWNT-TFTs as a function of solution sonication time. (A) Box and whisker diagram displaying the on (top, black) and off (bottom, gray) current for batch 1. (B). Box and whisker diagram displaying the on (top, black) and off (bottom, gray) current for batch 2. The bounds of the boxes represent the 75th and 25th percentiles of the data set, the outer whiskers show the 95th and 5th percentiles and inner line represent the mean. Data presented are obtained from 9 to 13 transistor devices from the same wafer. (C) On/off ratio calculated from logarithmic averages of the data presented in A and B showing a degradation in transistor behavior with increasing sonication time.

longer sonication times, more defects would occur on the smaller diameter arc-discharge metallic SWNTs resulting in a decrease in the efficacy of self-sorting and an increase in the off current.

The second regime is dominated by the decreased concentration of SWNTs in solution and density on the surface. After 180 min, both the on and off currents decreased as a result of more SWNTs centrifuged out after water induced bundling. There is less percolation and an increased spread in distribution, especially in the off current, where there is a very low density of metallic SWNTs and little chirality control from surface sorting because of the sonication induced defects. The charge carrier mobility also had a significant change in this regime and decreased by two orders of magnitude as shown in Figure SI-5 in the Supporting Information. It should be noted that the devices from longer sonication times (batch 2, 420, and 480 min) did not have adequate SWNT surface density for percolation and resulted in insulating devices.

CONCLUSION

We show that changing the solution processing conditions for surface-sorted SWNT transistors changes the properties of the solution, length of SWNTs, and the metallic and semiconducting ratio of SWNTs adsorbed on the surface. For optimal SWNT transistor networks with high on/off ratios, and long unbundled SWNTs, a short (10 min) sonication time is required. However, comparable length distributions and good transistor performance with increased solution concentration can be obtained with slightly longer times up to 40 min. Even longer sonication times reduce the lengths of the SWNTs and degrade the on/off ratio of surface-sorted SWNT networks by introducing defects, shortening the SWNTs, and degrading the NMP solvent. These changes affect the device properties of the final transistor network. Understanding of the SWNT dispersion conditions is critical to the optimized performance of electronic devices.

Acknowledgment. We acknowledge support from the Stanford Global Climate and Energy Program and National Science Foundation ECCS 0901414. MCL acknowledges support from the IC postdoctoral fellowship. RR acknowledges the support from the National Science Foundation REU program from the Center for Polymer Interfaces and Macromolecular Assemblies (Grant Number 0648768). We also acknowledge Justin Opatkiewicz for editing assistance and technical discussions.

Supporting Information Available: (1) The effect of sonication on NMP in ambient conditions. (2) The average length of SWNTs as a function of sonication time. (3) Characteristic *I*−*V* plots for various sonication times. (4) Length and bundle distribution for batch 2. (5) Mobility as a function of sonication time for batch 2. (6) Additional AFM images (PDF). This material is available free of charge via the Internet at http://pubs.acs.org.

REFERENCES AND NOTES

(1) Cao, Q.; Rogers, J. A. *Adv. Mater.* **2009**, *21* (1), 29–53.
(2) LeMieux, M. C.; Roberts, M.; Barman, S.; Jin, Y. W.; Kim, J. M.; Bao, Z. N. *Science* **2008**, *321* (5885), 101–104.
(3) Bo, X. Z.; Lee, C. Y.; Strano, M. S.; Goldfinger, M.; Nuckolls, C.; Blanchet, G. B. *Appl. Phys. Lett.* **2005**, *86* (18), 182102.
(4) Hellstrom, S. L.; Lee, H. W.; Bao, Z. N. *ACS Nano* **2009**, *3* (6), 1423–1430.
(5) Futaba, D. N.; Hata, K.; Yamada, T.; Hiraoka, T.; Hayamizu, Y.; Kakudate, Y.; Tanaike, O.; Hatori, H.; Yumura, M.; Iijima, S. *Nat. Mater.* **2006**, *5* (12), 987–994.
(6) Kong, J.; Franklin, N. R.; Zhou, C. W.; Chapline, M. G.; Peng, S.; Cho, K. J.; Dai, H. J. *Science* **2000**, *287* (5453), 622–625.
(7) Star, A.; Joshi, V.; Skarupo, S.; Thomas, D.; Gabriel, J. C. P. *J. Phys. Chem. B* **2006**, *110* (42), 21014–21020.

(8) Snow, E. S.; Perkins, F. K.; Houser, E. J.; Badescu, S. C.; Reinecke, T. L. *Science* **2005**, *307* (5717), 1942–1945.
(9) Zhongfan, L.; Liying, J.; Yagang, Y.; Xiaojun, X.; Jin, Z. *Adv. Mater.* **2010**, *22*, 2285–2310.
(10) Snow, E. S.; Novak, J. P.; Lay, M. D.; Houser, E. H.; Perkins, F. K.; Campbell, P. M. *J. Vac. Sci. Technol. B* **2004**, *22* (4), 1990–1994.
(11) Hong, S.; Myung, S. *Nat. Nanotechnol.* **2007**, *2* (4), 207–208.
(12) Kang, S. J.; Kocabas, C.; Ozel, T.; Shim, M.; Pimparkar, N.; Alam, M. A.; Rotkin, S. V.; Rogers, J. A. *Nat. Nanotechnol.* **2007**, *2* (4), 230–236.
(13) Ishikawa, F. N.; Chang, H.-k.; Ryu, K.; Chen, P.-c.; Badmaev, A.; Gomez De Arco, L.; Shen, G.; Zhou, C. *ACS Nano* **2008**, *3* (1), 73–79.
(14) Cao, Q.; Kim, H. S.; Pimparkar, N.; Kulkarni, J. P.; Wang, C. J.; Shim, M.; Roy, K.; Alam, M. A.; Rogers, J. A. *Nature* **2008**, *454* (7203), 495–U4.
(15) Ding, L.; Tselev, A.; Wang, J. Y.; Yuan, D. N.; Chu, H. B.; McNicholas, T. P.; Li, Y.; Liu, J. *Nano Lett.* **2009**, *9* (2), 800–805.
(16) Arnold, M. S.; Green, A. A.; Hulvat, J. F.; Stupp, S. I.; Hersam, M. C. *Nat. Nanotechnol.* **2006**, *1* (1), 60–65.
(17) Engel, M.; Small, J. P.; Steiner, M.; Freitag, M.; Green, A. A.; Hersam, M. C.; Avouris, P. *ACS Nano* **2008**, *2* (12), 2445–2452.
(18) Wang, C.; Zhang, J.; Ryu, K.; Badmaev, A.; De Arco, L. G.; Zhou, C. *Nano Lett.* **2009**, *9* (12), 4285–91.
(19) LeMieux, M. C.; Sok, S.; Roberts, M. E.; Opatkiewicz, J. P.; Liu, D.; Barman, S. N.; Patil, N.; Mitra, S.; Bao, Z. *ACS Nano* **2009**, *3* (12), 4089–4097.
(20) Bahr, J. L.; Mickelson, E. T.; Bronikowski, M. J.; Smalley, R. E.; Tour, J. M. *Chem. Commun.* **2001**, (2), 193–194.
(21) Coleman, J. N. *Adv. Funct. Mater.* **2009**, *19* (23), 3680–3695.
(22) Moore, V. C.; Strano, M. S.; Haroz, E. H.; Hauge, R. H.; Smalley, R. E.; Schmidt, J.; Talmon, Y. *Nano Lett.* **2003**, *3* (10), 1379–1382.
(23) Zheng, M.; Jagota, A.; Semke, E. D.; Diner, B. A.; McLean, R. S.; Lustig, S. R.; Richardson, R. E.; Tassi, N. G. *Nat. Mater.* **2003**, *2* (5), 338–342.
(24) Lee, H. W.; You, W.; Barman, S.; Hellstrom, S.; LeMieux, M. C.; Oh, J. H.; Liu, S.; Fujiwara, T.; Wang, W. M.; Chen, B.; Jin, Y. W.; Kim, J. M.; Bao, Z. A. *Small* **2009**, *5* (9), 1019–1024.
(25) Zhang, Y. J.; Shen, Y. F.; Li, J. H.; Niu, L.; Dong, S. J.; Ivaska, A. *Langmuir* **2005**, *21* (11), 4797–4800.
(26) Zhou, W.; Vavro, J.; Guthy, C.; Winey, K. I.; Fischer, J. E.; Ericson, L. M.; Ramesh, S.; Saini, R.; Davis, V. A.; Kittrell, C.; Pasquali, M.; Hauge, R. H.; Smalley, R. E. *J. Appl. Phys.* **2004**, *95* (2), 649–655.
(27) Strano, M. S.; Dyke, C. A.; Usrey, M. L.; Barone, P. W.; Allen, M. J.; Shan, H. W.; Kittrell, C.; Hauge, R. H.; Tour, J. M.; Smalley, R. E. *Science* **2003**, *301* (5639), 1519–1522.
(28) Banerjee, S.; Hemraj-Benny, T.; Wong, S. S. *Adv. Mater.* **2005**, *17* (1), 17–29.
(29) Ausman, K. D.; Piner, R.; Lourie, O.; Ruoff, R. S.; Korobov, M. *J. Phys. Chem. B* **2000**, *104* (38), 8911–8915.
(30) Giordani, S.; Bergin, S. D.; Nicolosi, V.; Lebedkin, S.; Kappes, M. M.; Blau, W. J.; Coleman, J. N. *J. Phys. Chem. B* **2006**, *110* (32), 15708–15718.
(31) Bergin, S. D.; Nicolosi, V.; Streich, P. V.; Giordani, S.; Sun, Z. Y.; Windle, A. H.; Ryan, P.; Niraj, N. P. P.; Wang, Z. T. T.; Carpenter, L.; Blau, W. J.; Boland, J. J.; Hamilton, J. P.; Coleman, J. N. *Adv. Mater.* **2008**, *20* (10), 1876.
(32) O'Connell, M. J.; Bachilo, S. M.; Huffman, C. B.; Moore, V. C.; Strano, M. S.; Haroz, E. H.; Rialon, K. L.; Boul, P. J.; Noon, W. H.; Kittrell, C.; Ma, J. P.; Hauge, R. H.; Weisman, R. B.; Smalley, R. E. *Science* **2002**, *297* (5581), 593–596.
(33) Hecht, D.; Hu, L. B.; Gruner, G., *Appl. Phys. Lett.* **2006**, *89* (13), 133112.
(34) Heller, D. A.; Barone, P. W.; Strano, M. S. *Carbon* **2005**, *43* (3), 651–653.
(35) Sun, Z.; O'Connor, I.; Bergin, S. D.; Coleman, J. N. *J. Phys. Chem. C* **2009**, *113* (4), 1260–1266.
(36) Poulain, L.; Monod, A.; Wortham, H. *J. Photochem. Photobiol. A, Chem.* **2007**, *187* (1), 10–23.
(37) Li, W. Y.; Suelves, I.; Lazaro, M. J.; Zhang, S. F.; Morgan, T. J.; Herod, A. A.; Kandiyoti, R. *Fuel* **2004**, *83* (2), 157–179.
(38) Sun, X.; Zaric, S.; Daranciang, D.; Welsher, K.; Lu, Y.; Li, X.; Dai, H. *J. Am. Chem. Soc.* **2008**, *130* (20), 6551–6555.
(39) Landi, B. J.; Ruf, H. J.; Worman, J. J.; Raffaelle, R. P. *J. Phys. Chem. B* **2004**, *108* (44), 17089–17095.
(40) Kocabas, C.; Pimparkar, N.; Yesilyurt, O.; Kang, S. J.; Alam, M. A.; Rogers, J. A. *Nano Lett.* **2007**, *7* (5), 1195–1202.
(41) Topinka, M. A.; Rowell, M. W.; Goldhaber-Gordon, D.; McGehee, M. D.; Hecht, D. S.; Gruner, G. *Nano Lett.* **2009**, *9* (5), 1866–1871.
(42) Pike, G. E.; Seager, C. H. *Phys. Rev. B* **1974**, *10* (4), 1421–1434.
(43) Opatkiewicz, J. P.; LeMieux, M. C.; Bao, Z. N. *ACS Nano* **2010**, *4* (2), 1167–1177.
(44) Shen, L. X.; Li, J. *Phys. Rev. B* **2005**, *71* (16), 035412.

AM1005223